Galli P., Giaccio B. and Messina P.;2010:*The 2009 central Italy earthquake seen through 0.5 Myr-long tectonic history of the L'Aquila faults system*. Quaternary Science Reviews, **29**, 3768-3789.

Gaudiosi I., Del Monaco F., Milana G. and Tallini M.; 2013: *Site effects in the Aterno River Valley (L'Aquila, Italy): comparison between empirical and 2D numerical modeling starting from April 6th 2009 MW 6.3 earthquake*. Bulletin of Earthquake Engineering,**12**:, 697-716.

GEMINA;1962: *Ligniti e torbe dell'Italia continentale*. ILTE Ed. Torino, 319 pp.

Gosar A. and Lenart A.; 2010:*Mapping the thickness of sediments in the Ljubljana Moor basin (Slovenia) using microtremors*. Bulletin of Earthquake Engineering,**8**, 501–518.

Gruppo di Lavoro MS–AQ; 2010:*Microzonazione sismica per la ricostruzione dell'area aquilana*. Regione Abruzzo - Dipartimento della Protezione Civile, L'Aquila, 3 vol. and Cd-rom.

Ibs-von Seht M. and Wohlenberg J.; 1999:*Microtremor measurements used to map thickness of soft sediments*. Bull. Seismol. Soc. Am.,**89**, 250–259.

Improta L., Villani F., Bruno P.P., Castiello A., De Rosa D., Varriale F., Punzo M., Brunori C.A., Civico R., Pierdominici S., Berlusconi A. and Giacomuzzi G.; 2012: *High-resolution controlled-source seismic tomography across the Middle Aterno basin in the epicentral area of the 2009, Mw 6.3, L'Aquila earthquake (central Apennines, Italy)*. Ital. J. Geosci. (Boll. Soc. Geol. It.), **131**, 373-388.

Konno K. and Ohmachi T.; 1998: *Ground motion characteristics estimated from spectral ratio between horizontal and vertical components of microtremor*. Bull Seism Soc Am,**88**, 228–241.

Lanzo G., Tallini M., Milana G., Di Capua G., Del Monaco F., Pagliaroli A. and Peppoloni S.; 2011: *The Aterno Valley strong-motion array: seismic characterization and determination of subsoil model*. Bull Earthquake Eng,**9**, 1855–1875.

Lunedei E. and Albarello D.; 2010: *Theoretical HVSR curves from full wavefield modelling of ambient vibrations in a weakly dissipative layered Earth*. Geophys. J. Int., **181**, 1093–1108.

Milana G., Azzara R.M., Bertrand E., Bordoni P., Cara F., Cogliano R., Cultrera G., Di Giulio G., Duval A.M., Fodarella A., Marcucci S., Pucillo S., Régnier J. and Riccio G.; 2011: *The contribution of seismic data in microzonation studies for downtown L'Aquila*. Bull. Earthquake Eng., **9**, 741–759.

Mucciarelli M.; 1998:*Reliability and applicability of Nakamura's technique using microtremors: an experimental approach*. J. Earthquake Engin., **2**, 625-638.

Nakamura Y.; 1989:*A method for dynamic characteristics estimation of subsurface using microtremor on the ground surface*. QR Railway Tech. Res. Inst.,**30**, 25–33.

SESAME; 2004:*Guidelines for the implementation of the H/V spectral ratio technique on ambient vibrations—measurements, processing and interpretations*. SESAME European research project EVG1-CT-2000-00026, deliverable D23.12.

Tallini M., Cavuoto G., Del Monaco F., Di Fiore V., Mancini M., Caielli G., Cavinato G.P., De Franco R., Pelosi N. and Rapolla A.; 2012:*Seismic surveys integrated with geological data for in-depth investigation of Mt. Pettino active Fault area (Western L'Aquila Basin)*. Ital. J. Geosci. (Boll. Soc. Geol. It.) **131**, 389-402.

2-D MODELING OF TOPOGRAPHIC EFFECTS USING THREE BASIC GEOMETRIES AND THE SPECTRAL-ELEMENT METHOD

G. Di Giulio
Istituto Nazionale di Geofisica e Vulcanologia, L'Aquila, Italy

Topographic effect. In the present work, the topographic effect was investigated selecting three basic 2-D geometries and using the feasibility of the spectral-element method (SEM; as implemented in the *specfem2d* code). The 2-D geometries were a triangle, an half-circle and a slope. 2-D models (P-SV waves) considering a real topography (Mount Ocre in L'Aquila district) were also performed, varying the velocities and the number of nearby topographic peaks.

Indeed it is known that jointly with local soil condition, geometrical morphological irregularities (slope, ridge, canyon, cliff, etc.) can amplify the seismic ground motion during earthquakes. Topographic site effects depends strongly on the geometry, on input wave

and location of receivers (Paolucci *et al.,* 2002; Pagliaroli, 2006; Hailemikael, 2010 for an overview). Topographic effect on rock sites is difficult to decouple from other amplification effects, such as surface layering/weathering, cracking of the bedrock, presence of faults, and directivity of the source. For these reasons, seismic and geological experiments at topographic sites are important because can provide information on the local velocity structure.

Numerical simulations available in literature agree in showing complex amplification/deamplification patterns, caused by interaction of elastic waves with the surface curvature. The maximum level of amplification occurs when the incident wavelength is comparable to the horizontal dimension of the topographic irregularities. As first approximation, the amplification increases as the average slope of the modeled geometry becomes steeper; for incidence not vertical, the area of largest amplification shifts in opposite direction with comparison to the propagation direction.

Experimental studies on topographic sites are mainly based on analysis of earthquake and noise data collected by several receivers, aimed at following ground-motion variation along the topography. The methods of analysis include mostly standard spectral ratio using a reference-site (SSR), single-station method (horizontal-to-vertical spectral ratio, HVSR), polarization and array analysis (Spudich *et al.,* 1986 among many others). Topographic amplification is often associated to a ground-motion polarization, observed both on noise and earthquake recordings (Marzorati *et al.,* 2011; Burjánek *et al*. 2012a, 2012b; Pischiutta *et al.,* 2013). Although the cause of polarization is still debated, largest amplification seems to appear in transverse direction to the main topography elongation (see also the recent NERA-JRA1 project, WP11, Waveform modeling and site coefficients for basin response and topography, Responsible activity leader P.Y. Bard, ftp://www.orfeus-eu.org/pub/NERA/Deliverables/).

The amplification caused by topography is usually expressed by the topographic aggravation factor (*TAF*) in the time or frequency domain. *TAF* is defined as the ratio between some ground motion parameters (PGA, PGV, PGD, Fourier amplitude spectra, response acceleration spectra etc) of a receiver along the topographic profile and the same parameter measured at an "ideal" free-field site. *TAF* is equivalently expressed as the ratio between ground motion amplification (*X*) related to 2-D (and/or 3-D) effects, and the stratigraphic amplification at the same site related to 1-D effects:

$$TAF = X(2\text{-}D)/X(1\text{-}D)$$

Numerical and experimental studies indicate the topographic effect as depending on the frequency, but European seismic design code (EC8; CEN2008) provides a topographic coefficient (*St*) frequency-independent. *St* is only depending from the steepness of the slope and the geometry of the topographic sites. The same approach follows the Italian building code (NTC08), which takes into account four classes of topographic categories (T1, T2, T3 and T4) with St ranging from 1 to 1.4; design elastic spectra are uniformly multiplied by St coefficient to include the topographic effect.

2-D SEM Modeling of "basic geometries". The spectral-element method (SEM) (as implemented in the *specfem2d* code https://geodynamics.org/cig/software/specfem2d/; Komatitsch and Vilotte, 1998; Chaljub *et al.,* 2007) was used for studying the effect of three basic 2-D geometries. The specific of the SEM is in the combined use of high-order Legendre polynomials and of the Gauss-Lobatto-Legendre (GLL) quadrature rule to evaluate the integrals within the weak (or variational) formulation of the equation of motion (see Fichtner 2011 for an extensive overview).

P-SV models were computed using the following irregular geometries: an half-circular hill (diameter 600 m), a triangular ridge (with dimension 600·300 m for base and height, respectively), and a slope with dip of 45° (dimension 300·300 m for base and height, respectively).

The 2-D models were subjected to a vertical incidence of planar waves (Fig. 1); the seismic input is a Ricker pulse with a central frequency of 5 Hz exciting the model approximately from

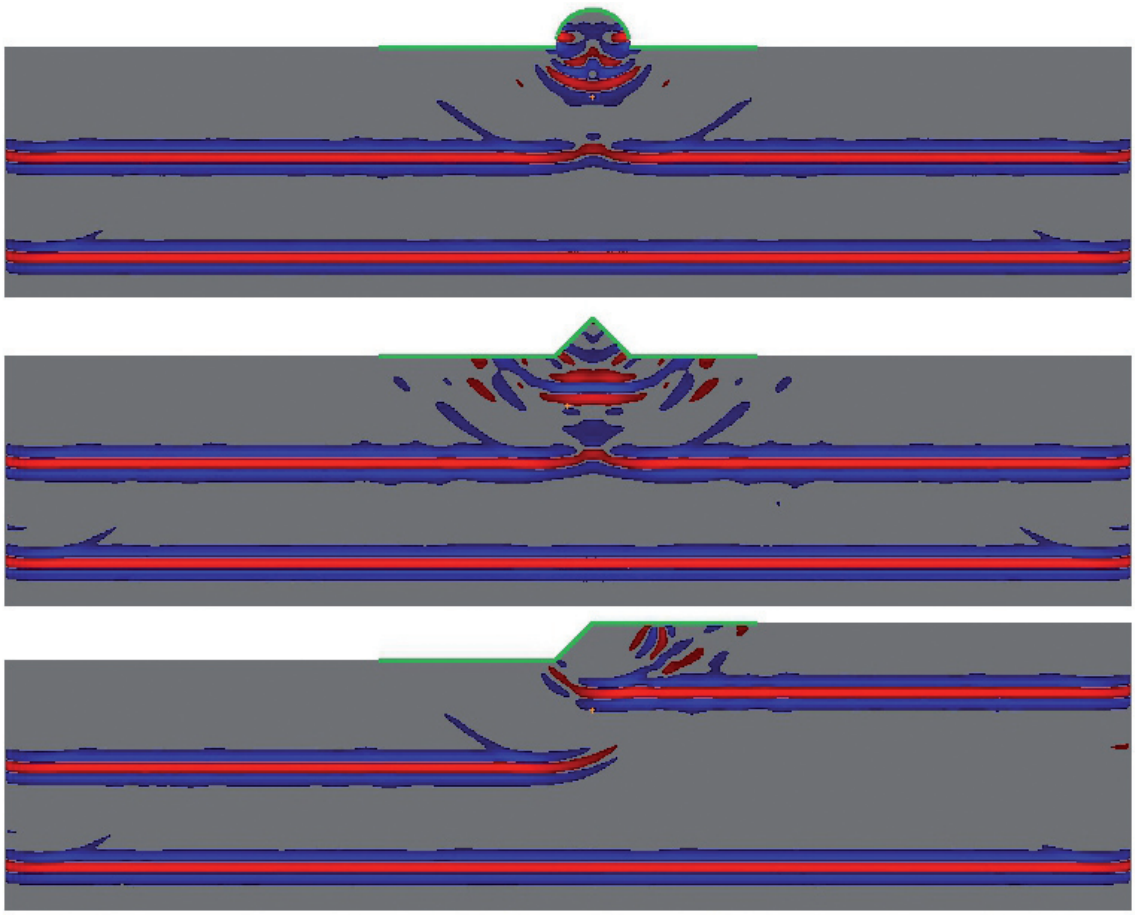

Fig. 1 – Basic geometries used in the 2-D P-SV modeling: half-circle, slope and triangle. A planar up-going and down-going Ricker wave is propagating into the model (*specfem2d* tool). Red and blue colors indicate the negative and positive pulse of seismic wave, respectively. The plot refers to S source polarization, and the snapshots correspond to a time step of 1.5 sec after the beginning of the simulation.

1 to 10 Hz. P- and S- input polarizations were kept separately; first I ran a modeling with a S- source input polarization, then I repeated the computation using a P- source polarization. The output synthetics computed along the surface contain both the polarization (P- and S-waves) due to the interferences between input pulse and waves diffracted from the irregular geometries.

I used the internal mesher of *specfem2d* respecting the time and spatial discretization rules, obtaining 270000 reference rectangular elements and 4324801 grid points for each single model mesh. The left, right and bottom sides of each model were absorbing boundaries using on the whole about 6000 PML (Perfectly Matched Layers) spectral elements, with mean thickness of the absorbing layer around 30 m. Accordingly, the spurious waves generated from the boundaries show negligible energy. The compressional (Vp) and shear-wave velocity (Vs) of the models were fixed to 2000 and 1000 m/s, respectively. The quality factors Q for P- and S- waves were assumed to be 200 (damping of 0.25%) and 100 (damping of 0.5%), following the usual (velocity/10) rule of thumb. The density was fixed to 2 g/cm^3 and the Poisson's ratio was 0.33. The computational dimension of each model was 9000·2000 m (x and z direction, respectively). The receivers were in number of 250 and were situated along the uppermost surface, with a spacing between adjacent receivers of about 12 m.

The snapshots at different time steps (Fig. 1) and the stack of the signal traces show clearly the effect of irregular geometries on the seismic waves. The half-circle, the slope and the triangle distort the planar input, acting as diffractors of energy and generating waves diffracted from the geometrical irregularities propagating along the surface. On the left- and right- part from the basic geometries, the waves travel symmetrically along the flat surface. The symmetry of

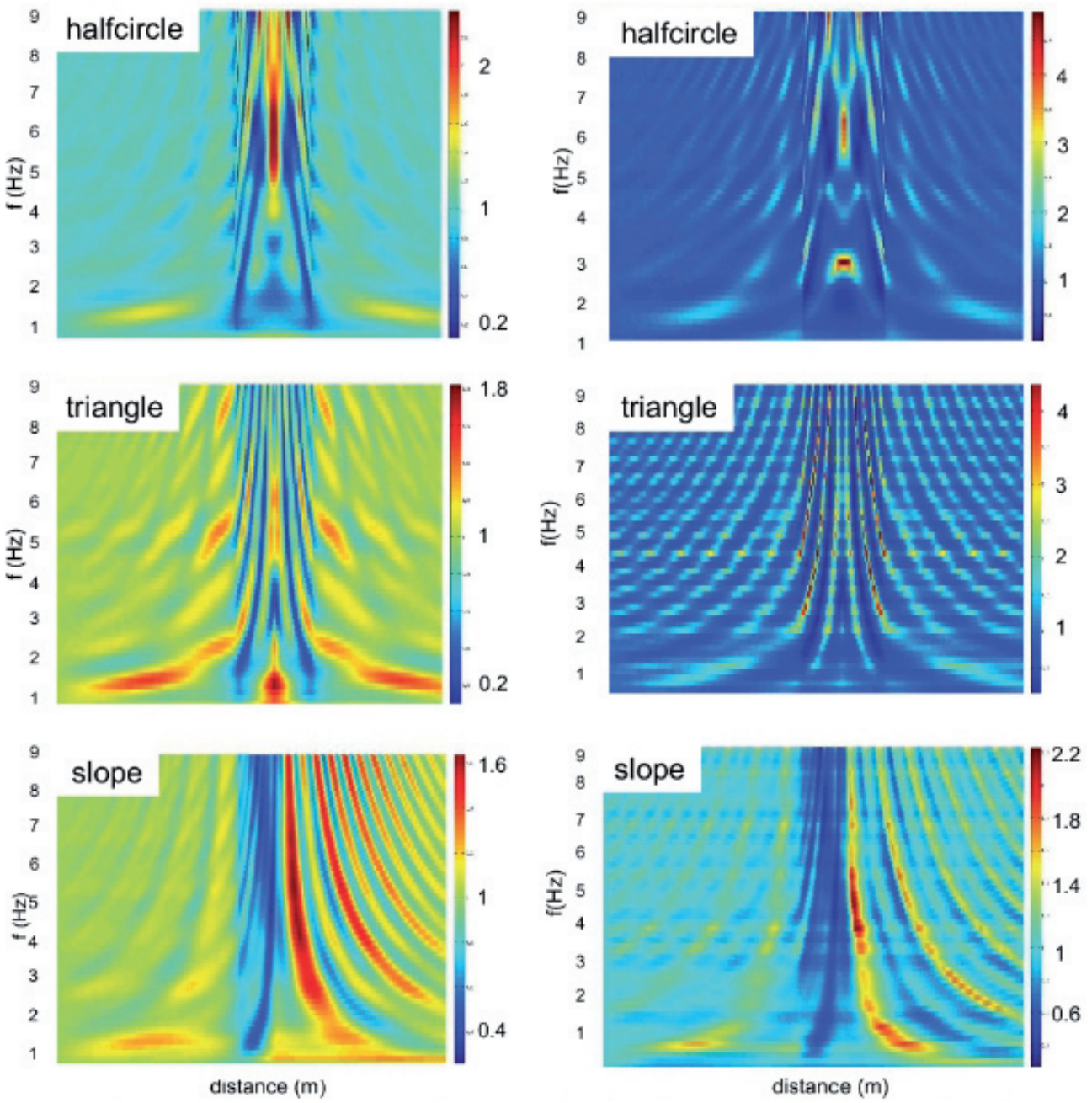

Fig. 2 – Left panel) SSR computed on synthetics for the half-circle, triangle and slope geometry. The plot refers to x component in case of S input polarization. The color scale is proportional to the SSR amplitude. Right panel) HVSR computed on synthetics for the half-circle, triangle and slope geometry. The color scale is proportional to the HVSR amplitude. HVSR was computed as (H/Href)/(V/Vref); see text.

the waves propagation is lost for the slope geometry (Fig. 1); the later arrivals on the right- part of the model (at higher elevation) show larger amplification rather than the left- part (at lower elevation).

The synthetic signals have been used to compute the standard spectral ratio (SSR), choosing as reference site the first receiver (number #1 located at x progressive of 1000 m) situated on the left part of the model. The output signal at each receiver was decimated (downsampling at 100 Hz with an antialiasing filter) and processed by means of a discrete Fourier Transform after removing the mean. The Fourier amplitude spectra (FAS) were subjected to a smoothing arithmetic algorithm. Finally for homologous components, the ratio of the FAS of the signal at each receiver over the FAS of the reference receiver was computed.

SSR for the x and z component is shown in Fig. 2 (left panel) indicating a complex pattern with alternate multitudes of amplification and deamplification branches. The maximum

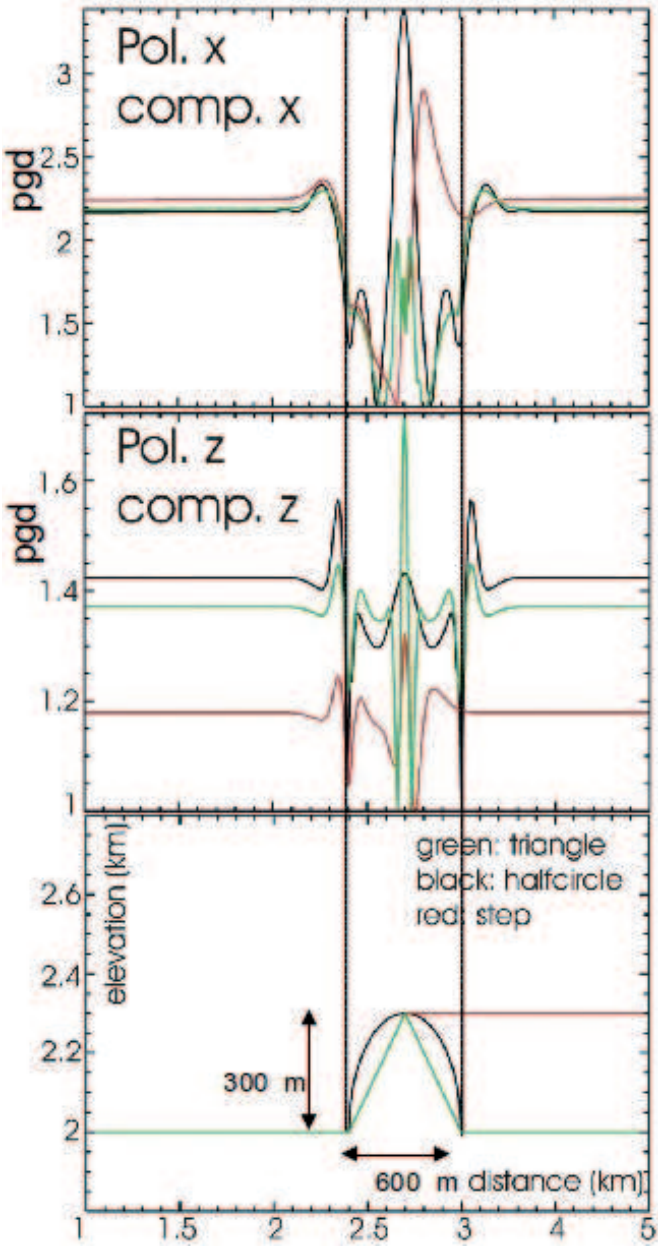

Fig. 3 – Normalized PGD along the surface of the three geometries. Red, green and black curves show the slope, the triangle and the half-circle (bottom panel). Top panel shows the PGD trend for x component and S input polarization; middle panel shows the PGD trend for z component and P input polarization.

amplification level of SSR is about 2. For vertical incidence of planar waves, the half-circle and the triangle show obviously a symmetric behavior, even if differences in the occurrence of maxima and minima of SSR can be observed between the half-circle and the triangle. As also shown by the time series, the slope-like shape displays larger SSR amplification in the right part of the model settled at higher elevation, whereas deamplified SSR values (blue color in Fig. 2) are evident at the midpoint of the x-axis which corresponds to the spatial position of the slope.

The synthetic signals have been also used to compute the horizontal-to-vertical spectra ratio (HVSR; Fig. 2). Because I kept separated the P- and S- polarization of the seismic input, the HVSR was computed as double ratio (H/Href)/(V/Vref); the term H/Href is the SSR in case of x component and S- input polarization, and the term V/Vref is the SSR computed on z component for P- input polarization. Fig. 2 (right panel) indicates a different pattern for the three geometries. The HVSR of the half-circle shows, in proximity of the uppermost vertex, strong resonance at about 2.5 and 6 Hz with amplitudes around 4. The HVSR of the triangle shows deamplification at the vertex position. Narrow patterns of amplification and deamplification start from the flank of the triangular ridge up to the flat part of the model. The HVSR of the slope still shows larger amplification in the right part of the model located at higher elevation. The maximum levels of HVSR value are 4.5 for the half-circle and the triangle, and 2.2 for the slope (Fig. 2 right panel).

The output synthetics are also used to provide insights on the topographic aggravation factor (TAF). According to the previous definition, the comparison between peak ground displacement (PGD) measured at a target receiver and PGD measured at an "ideal" site not affected by topography can be related to TAF. The distribution of PGD computed from synthetics along the topographic profile is illustrated in Fig. 3, where the PGD minima of the three geometries were normalized to 1. The receiver number #1 (placed at a progressive x of 1000 m) is accepted as "ideal" free-field site. The distributions of peak ground velocity and acceleration (PGV and PGA) were also computed after single (or double) differential of the displacement time-series, obtaining very similar trend to the PGD one.

Fig. 3 shows that the increase (or decrease) of PGD is strongly depending by the geometrical shapes and source polarization. For x component and S- source polarization (top panel of Fig. 3), the PGD reaches the same level of minimum (with respect to receiver number #1) for all the

three modeled shapes. The plateau value decreases from a value of 2.2 up to 1 (approximately at the midpoint of the geometries). The PGD peak is largest for the half-circle (black curve in Fig. 3 top panel) with the maximum amplification occurring exactly at its uppermost vertex, whereas the triangle is mostly characterized by deamplification of the ground motion (green curve in Fig 3 top panel). The slope geometry (red curve in Fig. 3 top panel), in case of x component and S-source polarization, shows a PGD increase (from 2.2 in the plateau part to 2.9) with the largest amplification occurring in a narrow zone immediately after the slope (between 2800 and 2900 m), similar to a "damage belt zone" effect.

For z component and P- source polarization (middle panel of Fig. 3), the largest PGD peak is observed for the uppermost vertex of the triangle (green curve in Fig. 3 middle panel) with value from 1.4 (plateau part of the figure) to 1.9 (vertex). The uppermost vertex of the half-circle (black curve) in this case does not modify the PGD with respect to the plateau value, whereas rapid variations of amplification and deamplification appear near the base of the half-circle geometry. The slope (red curve in Fig. 3 middle panel) shows lower deviation between PGD maxima and PGD minima than the other geometries.

The effect of the topographic shapes on PGD, as observed in the Fig. 3 for both the polarization, starts from the progressive 2200 up to 3200 m (x axis), i.e. 200 m before and after the irregular shapes. This measurement (200 m) is comparable to the half-width (300 m) of the modeled shapes, therefore their effect seems to spatially extend for a length of the same order of the half-width of the topographical irregularities.

Case-study: Mount Ocre. After the 2-D simulation of P-SV waves propagating in simple irregular shapes, the realistic topographic profile of Mount Ocre (courtesy of Antonio Avallone) was modeled. Mount Ocre (about 9 km in SE direction from L'Aquila downtown) is interesting because it is available at this site a record of the Mw 6.1 L'Aquila mainshock (on April 6, 2009) acquired by a high-rate GPS station (site named CADO with a 10 Hz as sampling rate; Avallone *et al.,* 2014). CADO is on the crest of a narrow ridge, which is elongated in the NW-SE direction bounding the Aterno river valley. Following Avallone *et al.* (2014), the vertical component of L'Aquila mainshock recorded at CADO shows a maximum subsidence of about 18 cm, and the horizontal components show a strong nearly-harmonic high-amplitude 1 Hz phase. This harmonic phase shows a maximum peak-to-peak amplitude of 36.4 cm in the east component and 22.6 cm in the north component. The particle motion in the horizontal plane results in a maximum displacement of 42.8 cm in the N+60° clockwise direction, approximately normal both to the fault strike of the region and to the ridge elongation. The horizontal polarization at 1 Hz is assumed to be a site property because is independent from the nature of the source signal. Indeed using directional H/V ratios, the same polarization resulting from the mainshock was observed from noise measurements surrounding CADO, and also from local small-magnitude earthquakes recorded by a co-located seismic station (Avallone *et al.,* 2014). The outcropping rock at CADO is fractured and weathered limestone, but the observed strong site effect at 1 Hz is not consistent with the results of array experiments conducted within the aim of the NERA Project nearby CADO (Rovelli *et al.,* 2012).

The possible role of the topography at CADO has been investigated using a 2-D model with the following parameters: Vs=1000 and Vp=2000 m/s; Qs=100 and Qp=200; mass density fixed to 2.5 g/cm^3. For simplicity and because the analysis is focused on the amplification induced by the topographic profile, the relief is modeled as having uniform rock properties and the adjacent Aterno basin is not included in the model. The ground motion amplification at Mount Ocre was estimated using the SSR approach for synthetic waveforms with respect to a reference site. The reference site was the synthetic seismogram of the same model without topography. A P-SV computation, using a different code than *specfem2D*, was also performed at this site by means of a finite-element approach in time-domain (Caserta 1998; Caserta *et al.* 2002) which adopts a triangle mesh generator (http://www.cs.cmu.edu/~quake/triangle.html). However the SSR results of the two codes (*specfem2d* and Caserta code) were very similar up to 8 Hz.

SSRs at Mount Ocre show spectral behavior similar to the one discussed previously for the basic geometries, with multiple alternation of amplification and deamplification patterns. In proximity of the crest where CADO site is located, the 2-D simulation shows ground motion amplification at high frequency (f > 3 Hz) and the amplitude is smaller than a factor of 2 around 1 Hz. Although the modelling is very simple (2-D and uniform rock), the numerical predictions suggest that the peculiar high-amplitude wave train observed at 1 Hz cannot be reproduced by lateral variations of the topography. This is true also considering the effect of nearby topographic peaks assuming a longer profile in the x direction, or reducing the velocity values by a factor of 2. SSRs computed on synthetics still indicate that no realistic velocities give amplifications comparable to the observations when uniform rock models are adopted. Avallone *et al*. (2014) commented the amplification mechanism of CADO as related to wave-guide amplification phenomena of trapped waves within a low-velocity fault zone (LVFZ). The horizontal extension of the fault zone in proximity of CADO was estimated by these authors around 650 m, and the velocity reduction within the LVFZ was around 40% with respect to the surrounding quarter-spaces.

Conclusion. Topographic effects have been investigated from spectral-element P-SV simulations considering three basic geometries (Fig. 1). The geometrical irregularities, in case of vertically incident plane waves, generate lateral propagating surface pulses and distinct patterns of amplification and deamplification, with an amplitude level mostly below 2 for SSR or below 4.5 for HVSR (Fig. 2). The pattern of amplification/deamplification is different for the horizontal and vertical components, depending on the shapes of the modeled irregularities and on polarization of the seismic input.

The output synthetics allow also to provide insights on the topographic aggravation factor (*TAF*), which is computed as the ratio of peak ground displacements (PGD) using an ideal reference site. The *TAF* pattern clearly illustrates the alternate position of amplified and deamplified values along the profile (Fig. 3). The numerical simulations show that the effect on the PGD distribution spatially extends before and after the position of the basic geometries, for a length of the same order of the half-width of the topographical irregularities (Fig. 3). Further in case of the geometrical slope, the largest amplitudes of late pulse are found in the part of the model characterized by higher elevation.

Assuming the real topography of Mount Ocre, the polarized 1 Hz amplification cannot reproduced by simple models with homogeneous velocities and taking into account only the topography. As discussed in Avallone *et al*. (2014), the observed amplification is likely related to a fault-zone effect, indicating that more advanced simulations are necessary in understating topographic effects on rock sites.

Acknowledgments. Antonio Rovelli and Antonio Avallone are gratefully acknowledged. Their constructive comments and suggestions helped to improve this work.

References

Avallone A., Rovelli A., Di Giulio G., Improta L., Ben-Zion Y., Milana G. and Cara F.; 2014: *Waveguide effects in very high rate GPS record of the 6 April 2009, Mw 6.1 L'Aquila, central Italy earthquake*. J. Geophys. Res.: Solid Earth, 119(1), 490-501.

Burjánek J., Moore J.R., Yugsi Molina F.X. and Fäh D.; 2012a: *Instrumental evidence of normal mode rock slope vibration*. Geophys. J. Int., **188**(2), 559-569.

Burjánek J., Cauzzi C., Fäh D., Bard P.Y., Cornou C., Pitilakis K., Massa M., Theodulidis N. and Bertrand E.; 2012b: *Toward reliable characterization of sites with pronounced topography and related effects on ground motion*. 15 WCEE (World Conference Earthquake Engineering), Lisboa, Portugal.

Caserta A.; 1998: *A time domain finite-difference technique for oblique incidence of antiplane waves in heterogeneous dissipative media*. Annals of Geophysics, **41**(4), 617-631.

Caserta A., Ruggiero V. and Lanucara P.; 2002: *Numerical modelling of dynamical interaction between seismic radiation and near-surface geological structures: a parallel approach*. Computers & geosciences, **28**(9), 1069-1077.

CEN (Comité Européen de Normalisation) Eurocode 8; 2008: *Design of structures for earthquake resistance. Part 1: General rules, seismic actions and rules for buildings*.

Chaljub E., Komatitsch D., Vilotte J.P., Capdeville Y., Valette B. and Festa G.; 2007: *Spectral-Element analysis in seismology*. In R.-S. Wu and V. Maupin Editors. Advances in wave propagation in heterogeneous media, volume **48** of Advanced in Geophysics, pages 365-419, Elsevier-Academic Press, London, UK.

Fichtner A.; 2011: *Full seismic waveform modelling and inversion*. Advances in Geophysical and Environmental Mechanics and Mathematics, doi 10.10007/978-3-642-15807-0_4. Springer-Verlag Berlin Heidelberg 2011.

Hailemikael S.; 2010: *Ground motion amplification at rock sites as determined by empirical and numerical methods*. PhD Thesis, University La Sapienza, Rome, Italy.

Pagliaroli A.; 2006: *Studio numerico e sperimentale dei fenomeni di amplificazione sismica locale di rilievi isolati*. PhD Thesis, Università di Roma La Sapienza, Roma, Italy, in Italian.

Komatitsch D. and Vilotte J.P. ; 1998: *The spectral element method: an efficient tool to simulate the seismic response of 2D and 3D geological structure*. Bull. Seism. Soc. Am., **88**(2), 368-392.

Marzorati S., Ladina C., Falcucci E., Gori S., Saroli M., Ameri G. and Galadini F.; 2011: *Site effects "on the rock": the case of Castelvecchio Subequo (L'Aquila, central Italy)*. Bull. Earthquake Eng., **9**(3), 841-868.

NTC08; 2008: *Norme Tecniche per le Costruzioni*. DM 140108, Ministero delle Infrastrutture, Gazzetta Ufficiale n. 29, Rome, Italy.

Paolucci R.; 2002: *Amplification of earthquake ground motion by steep topographic irregularities*. Earth. Eng. Struct. Dyn., **31**, 1831-1853, doi:10.1002/eqe.192.

Pischiutta M., Rovelli A., Salvini F., Di Giulio G. and Ben-Zion Y.; 2013: *Directional resonance variations across the Pernicana Fault, Mt Etna, in relation to brittle deformation fields*. Geophys. J. Int., **193**(2), 986-996.

Rovelli A. *et al.*; 2012: *Geophysical surveys on basins and topographies: report and findings*. Deliverable D11.3 NERA-JRA1 project, WP11 Task 11.4, ftp://www.orfeus-eu.org/pub/NERA/Deliverables/NERA_D11.3.pdf.

Spudich P., Hellweg M. and. Lee H.K; 1996: *Directional topographic site response at Tarzana observed in aftershocks of the 1994 Northridge California earthquake: Implications for mainshocks motions*. Bull. Seismol. Soc. Am., **86**, 193-208.

LA MICROZONAZIONE SISMICA NEL CENTRO ABITATO DI FIVIZZANO (MS)

V. D'Intinosante[1], GDL-Fivizzano[2]

[1] Settore Sismica, Regione Toscana, Firenze, Italia

[2] Il GDL (Gruppo di Lavoro) Fivizzano: M. Baglione, V. D'Intinosante, F. Vannini, P. Fabbroni, L. Nistri (Settore Sismica, Regione Toscana); A. Puccinelli, G. D'Amato Avanzi (Dipartimento Scienze della Terra – Università di Pisa); G. Naso (Dipartimento della Protezione Civile Nazionale, Ufficio rischio sismico – Roma); G. Cavuoto, V. Di Fiore, N. Pelosi, M. Punzo, D. Tarallo (CNR– IAMC di Napoli); S. Piscitelli, A. Perrone, J. Bellanova, G. Calamita (CNR– IMAA di Potenza); M. Moscatelli, A. Pagliaroli, M. Simionato, D. Pileggi, A. Avalle (CNR– IGAG di Roma); G. Vessia (INGEO – Università di Chieti); G. Ginesi (Ufficio Cave e Ambiente – Comune di Fivizzano, MS)

Introduzione. La Regione Toscana ha avviato a partire dal 1997, il Programma di Valutazione Effetti Locali (denominato Programma VEL), finalizzato all'acquisizione di dati geologici, geotecnici e geofisici in corrispondenza dei principali centri abitati, ubicati nelle aree a maggior pericolosità sismica del territorio regionale (Ferrini *et al*., 2007).

In particolare, la gran mole di dati di prospezione diretta ed indiretta del sottosuolo (D'Intinosante *et al*., 2014), ha consentito la realizzazione di studi di microzonazione sismica di dettaglio (definita di "terzo livello" nell'ambito degli "Indirizzi e criteri per la microzonazione sismica", di seguito indicato con la sigla ICMS), fornendo un importante modello geologico-tecnico delle aree di studio, assolutamente necessario per analizzare in maniera analitica la risposta sismica locale a livello areale in assetto perlomeno bidimensionale.

Tali attività, afferenti al settore multidisciplinare della prevenzione sismica, sono previste in ambito regionale dalla L.R. 58/2009 comma 1b e vengono svolte attualmente nel rispetto dei criteri e delle modalità operative previsti dagli ICMS.

Mediante i finanziamenti erogati principalmente con l'OPCM 3907/2010 e s.m.e i. è stato possibile finalizzare gli studi di microzonazione sismica di terzo livello (anche definita MS3) nelle località riportate in Tab. 1. Ai centri abitati elencati in tabella, sono da aggiungere i Comuni